Available online at www.sciencedirect.com
SCIENCE DIRECT®
Journal of Power Sources 138 (2004) 68–78
JOURNAL OF POWER SOURCES
www.elsevier.com/locate/jpowsour

Modeling of catalyst layer microstructural refinement and catalyst utilization in a PEM fuel cell

Zoheir N. Farhat*

School of Manufacturing and Industrial Mechanical, British Columbia Institute of Technology-Polytechnic, Burnaby, BC, Canada V5G 3H2

Received 8 May 2004; accepted 30 May 2004
Available online 28 July 2004

Abstract

Polymer electrolyte membrane (PEM) fuel cell performance is largely controlled by the microstructure of the catalyst layer. Hence, a need exists to develop fundamental understanding of the effect of catalyst layer microstructure on a PEM fuel cell operational characteristics. Significant obstacles to commercialization of a PEM fuel cell have been attributed to high cost of the platinum catalyst, slow kinetics of the oxygen reduction reaction (ORR), and low catalyst utilization. In order to address these limiting factors, a model has been developed to investigate the effect of catalyst particle size, loading, utilization and distribution of catalyst layer components. The model predicts a large increase in the exchange current and in cell potential following a corresponding reduction in activation polarization as catalyst particle size decreases to a few nanometers. Model predictions compare well with published experimental data. The model also predicts an upper statistical limit of 22% to the amount of catalyst that can be utilized for current generation, even for best-prepared catalyst layer. This explains the observed low catalyst utilization (<25%) reported in the literature. In the proposed model, this statistical limit is attributed to the intrinsic characteristics of "randomly" distributed catalyst layer components. To achieve higher utilization, catalyst layer components must be distributed in an engineered design that ensures maximum number of active sites.

Keywords: Fuel cell; Catalyst layer; Modeling; Particle size; Catalyst utilization; Polarization

1. Introduction

High cost of the Pt catalyst and the slow kinetics of the O_2 reduction reaction process necessitated the search for alternative ways to concentrate the Pt catalyst in the catalyst layer of polymer electrolyte membrane (PEM) fuel cells. An effective method to lower the Pt loading without sacrificing performance is during the catalyst particle size to the nanoscale range, which effectively increases catalyst surface area available for current generation.

In recent years, nanocrystalline materials were the subject of extensive research and various techniques were developed to synthesize them [1–5]. These materials are polycrystalline in nature, but have an ultra-fine grain size of the order of 1–100 nm. In such materials the volume fraction of the grain boundaries becomes comparable to the volume fraction of the crystals themselves. As many as 50% of the atoms are located at interfacial boundaries. Due to this large volume fraction of grain boundaries, and the high surface area of these materials, they exhibit different properties than conventional engineering alloys [6].

Interest in nanostructured materials as potential catalysts is evident. The Literature shows that nanostructured catalysts exhibit improved catalytic activities [7–13]. However, because the processing and the application of nanostructures to catalysts is in its infancy, more work is needed to provide a fundamental understanding of this new class of catalysts. Along with experimental observation, theoretical modeling is needed to fully exploit microstructural parameters in an attempt to optimize fuel cell performance.

Several mathematical models have been proposed in the literature for PEM fuel cells; these models have concentrated on various aspects of PEM fuel cell operation, and their effect on cell performance. Models developed considered effects such as mass transport, porosity, gas pressures, water management, reaction kinetics, etc. A brief review of several of these models is given below.

Mann et al. [14] and Amphlett et al. [15] developed a parametric model of a single PEM cell by using a

* Tel.: +1 604 434 5734; fax: +1 604 303 8743.
E-mail address: zfarhat@bcit.ca (Z.N. Farhat).

0378-7753/$ – see front matter © 2004 Elsevier B.V. All rights reserved.
doi:10.1016/j.jpowsour.2004.05.055

mechanistic approach, and a number of grouped parameters were identified and fit to an empirical data measured from a Ballard Mark IV single cell. Similarly, Kim et al. [16] used an empirical equation to describe the performance data of a PEM fuel cell over a complete operating range. Grot et al. [17] and Fuller and Newman [18] incorporated strategies for thermal and water management. Marr and Li [19] extended Grot et al. model, and investigated catalyst utilization as well as the optimal composition and structure for the cathode catalyst layer; such as, catalyst loading, catalyst type, catalyst layer thickness, void fraction, and ionomer content. Springer et al. [20] developed an isothermal, one-dimensional, steady state model for water transport through a complete PEM fuel cell based on experimental results; their modeling results provided useful insight into the cell's water transport mechanisms and their effect on the cell performance. Bernardi and Verbrugge [21,22] developed a comprehensive mathematical model for a PEM fuel cell from fundamental transport properties. Nguyen and White [23] formulated a quasi-two-dimensional model to account for the variations of mass and heat transfer between the electrode and reactant gas mixture in the flow channel. Recently, Weisbrod et al. [24] presented a simplified through-the-electrode model, including water saturation and transport within the electrode and reaction kinetics within the cathode catalyst layer. Work of Lee et al. [25] presents the most comprehensive form of an empirical model produced to date to predict the current_voltage relationship for the typical PEM fuel cell. Gottesfeld and Zawodzinski [26] have also achieved considerable success in PEM fuel cell modeling over the last decade, resulting in increasingly complex predictors of cell performance based on interdependencies of process variables and the nature of transport processes. Eikerling and Kornyshev [27] proposed a phenomenological model that investigated the effect of O_2 diffusion, proton conduction and reaction kinetics in the catalyst layer. You and Liu [28] presented a pseudo-homogeneous model for the cathode catalyst performance in PEM fuel cell derived from the basic mass current balance by the control volume approach.

To date, a comprehensive model that directly relates catalyst layer microstructural refinement and catalyst utilization to PEM fuel cell performance is non-existent. The objective of this work is to develop a mathematical model relating catalyst structure refinement, loading, utilization and distribution to polarization effects and overall PEM fuel cell performance. In this paper, a modified expression for the exchange current in the Butler–Volmer equation is developed. The new expression incorporates a geometrical factor which includes both catalyst particle size and loading for a random distribution of catalyst layer components. Furthermore, a new parameter "utilization coefficient" has been introduced, which represents the fraction of catalyst surface area located in electrocatalytically active sites. The discussion in this paper may help in the optimization and design of cathode catalyst layer.

2. Model description

In this study the catalyst layer is assumed to consist of a mixture of catalyst platinum, ionomer membrane electrolyte, carbon support and void space (network of pores). Although the catalyst layer is relatively small, it is the heart of the fuel cell. Here fuel and oxidant react electrochemically to produce electrical energy. Four different media are present for the function of a catalyst layer: an interconnected solid phase of the carbon, which serves as the supplying network for the electrons; a network of gas pores, which supplies oxygen to the reaction sites; an electrolyte network provides the pathways for the protons to the catalyst places; and a catalytic surface for electrochemical reaction to take place (Fig. 1).

The performance of H_2/O_2 (fuel/oxidant) PEM fuel cell is limited primarily by the slow rate of the O_2 reduction half reaction, $O_2 + 4H^+ + 4e^- \rightarrow 2H_2O$, which is many more times slower than the H_2 oxidation, $2H_2 \rightarrow 4H^+ + 4e^-$. When current flows through a fuel cell, the potential drop due to polarization effect which is primarily controlled by the oxygen reduction reaction (ORR) rate.

In PEM fuel cell, the three-phase interface between the electrolyte, the electrode and the reactant gas (within a percolating network of ionomer, oxygen and electronic conducting medium) is important. Only catalyst located in this region is electrochemically active, i.e. capable of generating current. Clearly, the rate at which this happens will be proportional to the area of the electrode. Therefore, increasing the catalyst surface area by reducing catalyst particle size will give rise to increased reaction rates.

Previous models assume that the half-cell reaction has equal probability to occur anywhere on the electrode surface (apparent area). In PEM fuel cell, real area ≫ apparent area and not all electrode real area is available for reaction but only active sites are utilized for current generation. The exchange current, which reflects the activities of electrode, depends largely on the active surface area of the electrode. In this model, the exchange current in the Butler–Volmer

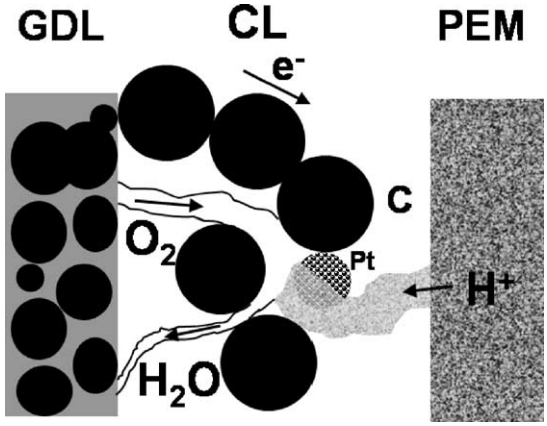

Fig. 1. Schematic diagram of an MEA illustrating the catalyst layer microstructure.

equation has been modified to include active surface area, which accounts for catalyst particle size, loading and utilization to give improved description of the electrode reaction kinetics.

3. Model formulation

Fuel cell potential as a function of polarization effects [29] for a single cell is given by:

$$E_{\text{cell}} = E_{\text{eq}} + \eta_{\text{c,act}} + \eta_{\text{a,act}} + \eta_{\text{c,conc}} + \eta_{\text{a,conc}} + \eta_{\text{ohmic}} \quad (1)$$

where E_{cell} is the irreversible measured voltage in the cell (when a net current passes through the circuit), E_{eq} is the Nernst equilibrium potential for the cell or reversible thermodynamic potential also known as open circuit voltage (OCV) (when no net current passes through circuit). $\eta_{\text{c,act}}$ and $\eta_{\text{a,act}}$ are cathode and anode activation overvoltages associated with kinetics limitations to the charge transfer process at the electrodes; $\eta_{\text{c,conc}}$ and $\eta_{\text{a,conc}}$ are concentration overvoltages resulting from depletion of reactants in the vicinity of the electrodes due to slow diffusion from bulk solution; and η_{ohmic} is the resistive overvoltage associated with the internal resistance in electrode, electrolyte and collectors. Experimental data to date on PEM fuel cells shows that the anode activation polarization is negligible with respect to the cathode activation polarization due to slow kinetics of the oxygen reduction reaction at the cathode.

Consider the following hypothetical half-cell electrode reaction (cathode reaction):

$$R + n_{\text{e}} \leftrightarrow P \quad (2)$$

The forward and backward reactions rates v_{f} and v_{b} (mol/cm^2 s), respectively, are as follows:

$$v_{\text{f}} = k_{\text{f}} C_{\text{R}} S = \frac{I_{\text{f}}}{nFA} \quad (3)$$

$$v_{\text{b}} = k_{\text{b}} C_{\text{P}} S = \frac{I_{\text{b}}}{nFA} \quad (4)$$

where k_{f} and k_{b} are the rate constants for the forward and the backward reactions in (cm^{-1} s^{-1}); C_{R} and C_{P} are reactant and product concentrations (mol/cm^3), respectively. In this model a parameter, S, is incorporated into the reaction rate expression, a "geometrical factor", that is a function of the catalyst layer microstructure (catalyst particle size, loading and utilization) and is equal to the total "active" surface area (cm^2). I_{f} and I_{b} are the forward (cathodic) and backward (anodic) current contributions to the total half-cell current in Amperes or Coulombs/s. A is the electrode nominal surface area (cm^2), F is Faraday constant (96,485 C/mol) and n is the stoichiometric number of electrons consumed in the electrode reaction. The need for a geometrical factor comes from the fact that, for PEM fuel cell, reaction takes place only at active sites within the catalyst layer and not at the entire real or nominal electrode surface areas. The net reaction rate is, therefore, the difference between forward and backward reaction rates, i.e.,

$$v_{\text{net}} = v_{\text{f}} - v_{\text{b}} = k_{\text{f}} C_{\text{R}} S - k_{\text{b}} C_{\text{P}} S = \left(\frac{I_{\text{f}}}{nFA}\right) - \left(\frac{I_{\text{b}}}{nFA}\right) \quad (5)$$

rearranging,

$$I_{\text{net}} = I_{\text{f}} - I_{\text{b}} = nFAS[k_{\text{f}} C_{\text{R}} - k_{\text{b}} C_{\text{P}}] \quad (6)$$

where I_{net} is the net half-cell current. Writing the rate constants as function of the standard rate constant (k°) and the half-cell overpotential ($E - E_{\text{eq}}$),

$$k_{\text{f}} = k^\circ \exp\left[\frac{-\alpha nF(E - E_{\text{eq}})}{RT}\right] \quad (7)$$

$$k_{\text{b}} = k^\circ \exp\left[\frac{(1-\alpha)nF(E - E_{\text{eq}})}{RT}\right] \quad (8)$$

where α is a charge transfer coefficient and E is the half-cell potential. Substituting Eqs. (7) and (8) into Eq. (6) and assuming no mass transfer effects (good convection), this yields a "modified" Butler–Volmer equation:

$$I = I_{\text{o}}\left[\exp\left(\frac{-\alpha nF\eta}{RT}\right) - \exp\left\{\frac{(1-\alpha)nF\eta}{RT}\right\}\right] \quad (9)$$

where η is the activation overpotential and is equal to $E - E_{\text{eq}}$, and I_{o} is a modified value for the exchange current:

$$I_{\text{o}} = nFASk^\circ C_{\text{R}}^{*(1-\alpha)} C_{\text{P}}^{*\alpha} \quad (10)$$

where C_{R}^* and C_{P}^* the are bulk concentrations of reactants and products, respectively. For the cathodic reaction where η is relatively large, the second term in Eq. (9) becomes negligible. Hence, the modified Butler–Volmer equation reduces to:

$$I = I_{\text{o}} \exp\left(\frac{-\alpha nF\eta}{RT}\right) \quad (11)$$

Dividing by the nominal area A and rearranging, then the activation polarization for the oxygen reduction reaction at the cathode will become:

$$\eta_{\text{c,act}} = \left(\frac{RT}{n\alpha_{\text{c}}F}\right) \ln\left(\frac{i_{\text{o,c}}}{i}\right) \quad (12)$$

where

$$i_{\text{o,c}} = nFSk^\circ C_{\text{O}_2}^{*(1-\alpha\text{c})} C_{\text{H}^+}^{*(1-\alpha\text{c})} C_{\text{H}_2\text{O}}^{*\alpha\text{c}} \quad (13)$$

Eq. (12) is known as Tafel equation and the term ($RT/n\alpha_{\text{c}}F$) is the Tafel slope. α_{c} represents the cathodic transfer coefficient, $C_{\text{O}_2}^*$, $C_{\text{H}^+}^*$ and $C_{\text{H}_2\text{O}}^*$ are the bulk concentrations of O_2, H^+ and H_2O in the PEM fuel cell, respectively. i is current density and $i_{\text{o,c}}$ is the modified exchange current density for the cathode reaction (oxygen reduction reaction on Pt catalyst).

3.1. Determination of the geometrical factor

Assuming that the catalyst layer consists of n_c randomly distributed spherical catalyst particle and that the single catalyst particle surface area is given by S_c (cm^2), then the total active surface area, S, is given by:

$$S = \gamma m_c S_c \tag{14}$$

where γ is a "utilization coefficient" which is the fraction of catalyst surface satisfying active area requirements for current generation (three-phase contact). That is, particles which are not in contact with the electronic conducting phase (catalyst and carbon support), electrolyte and/or gas percolating networks will not contribute to the active surface area and no current is generated from these areas. Substituting the surface area of a spherical particle of radius, r_c (cm), into Eq. (14), we get

$$S = 4\pi r_c^2 n_c \gamma \tag{15}$$

and the total volume of catalyst particles, V_c (cm^3), is given by:

$$V_c = \frac{m_c}{\rho_c} = \left(\frac{4}{3}\right)\pi r_c^3 n_c \tag{16}$$

where m_c (g) and ρ_c (g/cm^3) are the catalyst mass and density, respectively. Substituting n_c from Eq. (16) into Eq. (15), the active surface area becomes:

$$S = \frac{3\gamma m_c}{r_c \rho_c} \tag{17}$$

Now, substituting Eqs. (13) and (17) into Eq. (12):

$$\eta_{c,act} = \left(\frac{RT}{n\alpha_c F}\right) \ln\left(\frac{3\gamma m_c n F k^{\circ} C_{O_2}^{*(1-\alpha c)} C_{H^+}^{*(1-\alpha c)} C_{H_2O}^{*\alpha c}}{i r_c \rho_c}\right) \tag{18}$$

3.2. Determination of the "Utilization Coefficient"

Consider three sets of balls each has a different color, where n_w, n_b and n_r are the numbers of white, black and red balls, respectively. If you were to pick three balls from a randomly mixed set of $n_w + n_b + n_r$ balls, then the question is: what is the probability of picking one ball from each color? In contrast to our catalyst layer structure, where colors represent electrolyte, catalyst and gas regions, the question would become: what is the probability of finding the three regions in contact?

Therefore, a utilization coefficient (γ), in statistical terms, can be defined as the probability of having contact between catalyst (supported on an electronic conducting carbon network), electrolyte and gas in a randomly distributed constituents within the catalyst layer. Then γ can be calculated as follows:

$$\gamma = \frac{\binom{n_1}{r_1}\binom{n_2}{r_2}\binom{n_3}{r_3}}{\binom{n_t}{r_t}} = \frac{{}_{n_1}C_{r_1} \cdot {}_{n_2}C_{r_2} \cdot {}_{n_3}C_{r_3}}{{}_{n_t}C_{r_t}} \tag{19}$$

where ${}_nC_r$ is the number of ways in which r objects can be selected from a set of n distinct objects, also called the number of "combinations" and ${}_{n_t}C_{r_t}$ is the total number of combinations. For a catalyst layer Eq. (19) can be written as:

$$\gamma = \frac{{}_{n_e}C_1 \cdot {}_{n_c}C_1 \cdot {}_{n_s}C_1}{{}_{n_t}C_3} \tag{20}$$

where ${}_{n_c}C_1$ represents the number of combinations of finding one catalyst particle from a set of n_c catalyst particles, ${}_{n_e}C_1$ and ${}_{n_s}C_1$ are defined in a similar manner. ${}_{n_t}C_3$, gives the total number of combinations of finding three regions from a set of $n_t = n_e + n_c + n_s$. Although there are structural differences between the catalyst and the ionomer, it is reasonable to assume that at the contact zone electrolyte can be regarded as "particle-like" medium. γ given by Eq. (20) varies between 0 and 1 and represents the fraction of catalyst surface area that lies in the three-phase region. It should be emphasized that the above argument is valid only in a region above the percolation threshold. That is, assuming that the active sites (three-phase regions) have access to the electronic conduction path, oxygen pathway and an electrolyte network. Replacing γ in Eq. (18) by its value from Eq. (20), the modified activation polarization becomes:

$$\eta_{c,act} = \left(\frac{RT}{n\alpha_c F}\right) \ln\left(3\left\{\frac{{}_{n_e}C_1 \cdot {}_{n_c}C_1 \cdot {}_{n_s}C_1}{{}_{n_t}C_3}\right\} \times \frac{m_c n F k^{\circ} C_{O_2}^{*(1-\alpha c)} C_{H^+}^{*(1-\alpha c)} C_{H_2O}^{*\alpha c}}{i r_c \rho_c}\right) \tag{21}$$

Using analysis in reference [15], it can be shown that the concentration overpotential is given by:

$$\eta_{conc} = \left(\frac{RT}{nF}\right) \ln\left\{1 - \left(\frac{i}{i_l}\right)\right\} \tag{22}$$

where i_l known as the limiting current density for the electrode that has the lowest limiting current density. The limiting current density is the current at which the fuel is used up at a rate equal to its maximum supply speed. For the Ohmic polarization, potential drop is simply proportional to the current and is given by:

$$\eta_{ohmic} = ir \tag{23}$$

where r is the area specific resistance in the cell ($\Omega\,cm^2$).

Substituting all polarization effects (Eqs. (21)–(23)) into Eq. (1),

$$E_{\text{cell}} = E_{\text{eq}} - (i + i_n)r + \left(\frac{RT}{n\alpha_c F}\right) \times \ln\left(\left\{3\frac{[n_e C_1 \cdot_{n_c} C_1 \cdot_{n_s} C_1]}{n_t C_3} \times \frac{m_c nFk^{\circ} C_{O_2}^{*(1-\alpha c)} C_{H^+}^{*(1-\alpha c)} C_{H_2O}^{*\alpha c}}{(i + i_n)r_c \rho_c}\right\}\right) + \left(\frac{RT}{nF}\right) \ln\left\{1 - \left[\frac{(i + i_n)}{i_l}\right]\right\} \quad (24)$$

where i_n is a term added to account for the internal and fuel cross over equivalent-current density [30]. Eq. (24) gives the measured cell voltage as a function of catalyst particle size, loading and utilization for a randomly distributed constituents in the catalyst layer. E_{eq} can be calculated from the molar free energy of formation of H_2O, ΔG_f, using the relationship $E_{\text{eq}} = -\Delta G_f/nF$, where n is the number of electrons per each molecule of fuel consumed, this can also be determined from Nernst equation as a function of concentrations.

4. Results and discussion

The influence of different microstructural parameters in a catalyst layer can be studied, in depth, by examining model predictions given by Eq. (24). Substituting typical values [15,27,30–32] of the parameters in Eq. (24) for Pt catalyst:

$$E_{\text{cell}} = 1.2 - (i + 2)3 \times 10^{-5} + 0.06 \ln\left[\frac{9.37 \times 10^{-3} \gamma m_c}{r_c(i + 2)}\right] + 0.05 \ln\left\{1 - \left[\frac{i + 2}{900}\right]\right\} \quad (25)$$

where units for E_{cell}, i, m_c and r_c are volts, mA/cm^2, g and cm, respectively; γ is given by Eq. (20). A peak value of γ achieved, for a random mix, when the number of catalyst, gas and electrolyte regions are equal. Fig. 2 gives the value of γ as a function of the number of gas and electrolyte regions, for a constant value n_c of 10^3. It can be seen from this figure that when $n_e = n_s = n_c$ a spike appears which represents the highest γ value. Furthermore, for $n_e = n_s = n_c = n$, Fig. 3 reveals that for a large n (>100), the highest value of γ achievable is approximately 0.22. In other words, according to this model, only 22% or less of catalyst surface is available for current generation, since only particles in the three-phase region are electrochemically active. In the following discussion, a value of $\gamma = 0.22$, which is the most optimistic value of the "utilization coefficient", is used.

A crucial factor in improving fuel cell performance is therefore to increase the value of the exchange current, especially at the cathode. According to the model, the exchange current is highly influenced by catalyst particle size and loading. The log/log plot in Fig. 4 demonstrates the effect of catalyst particle size and loading on the exchange current. As the particle size is reduced from 1 μm to 1 nm, i_o increases by three orders of magnitude. The effect is due to a rapid increase in catalyst surface area, in particular, when r_c drops below 40 nm as illustrated in Fig. 5. Furthermore, for a given i_o, loading can be lowered from 100 to 0.1 mg/cm^2 provided that particle size is reduced from 0.5 mm to 15 nm. That is, lowering catalyst loading can be compensated for by using smaller catalyst particle size without effecting fuel cell performance.

The i–v characteristics in Fig. 6 reveal the dependence of fuel cell potential on catalyst particle size. The plot clearly shows how reducing catalyst particle size reduces overpotential and increases fuel cell voltage. Cell voltage rises

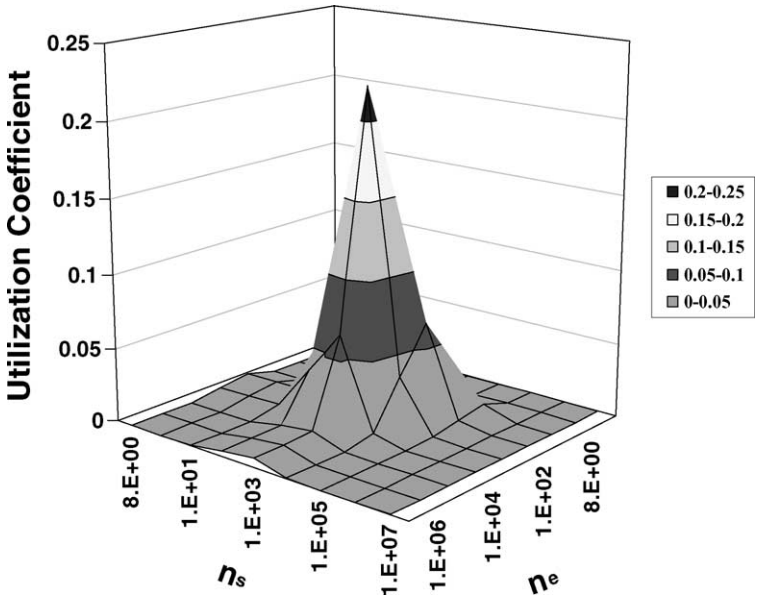

Fig. 2. Catalyst utilization coefficient as a function of n_e and n_s for $n_c = 10^3$.

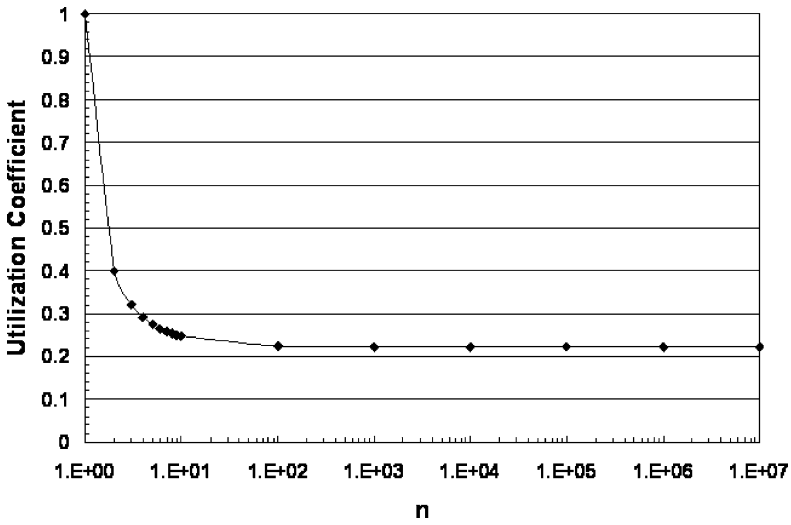

Fig. 3. Catalyst utilization coefficient vs. n, where $n = n_c = n_e = n_s$.

from 0.16 to 1.00 V as r_c decreases from 100 μm to 1 nm at 300 mA/cm^2. A similar behavior is observed when examining the effect of loading on cell performance (Fig. 7). As expected, for a given particle size, increasing catalyst loading has the effect of shifting the i–v plot towards higher potential. However, according to the model, higher cell specific power can be achieved when using lower catalyst loading (Fig. 8). The effect of catalyst particle size on % power loss (Fig. 9) shows significant increase in % potential loss accompanying the increase in catalyst particle size. Typical PEM fuel cell has loading of 0.5 mg/cm^2 and about 45% loss in potential at a current density of 300 mA/cm^2. It can be seen that, for the same potential loss of 45%, catalyst loading of 0.01 mg/cm^2 is possible if particle size is reduced to 2 nm, which is a large reduction in Pt cost.

The present model is tested against reported data published in the open literature. Table 1 compares fuel cell output potentials predicted from the model to published experimental values [33]. It clearly shows that the proposed model is in good agreement with experimental data. For various catalyst particle sizes and loadings, the differences between model predicted potentials and experimental results are in the range of 7.1–15.9%. The effect of catalyst particle size below 1 nm on the intrinsic electrocatalytic activities is controversial [37] as a consequence the present model is only valid above a 1 nm particle size.

The importance of catalyst utilization, represented in this model by the "utilization coefficient", γ, cannot be overemphasized. As mentioned above, in a random distribution of catalyst layer components, a maximum of 22% of components (catalyst, gas, and electrolyte) have direct contact, i.e., at best, only 22% of catalyst is utilized. In other words, the probability of having a Pt particle in active site is $\leq$22%. This upper "statistical" limit to the amount of catalyst

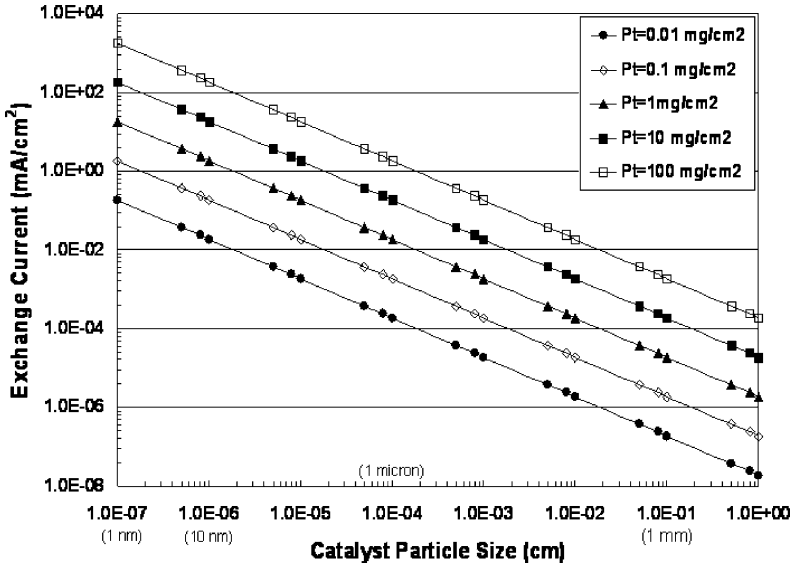

Fig. 4. The effect of the exchange current on catalyst particle size and loading.

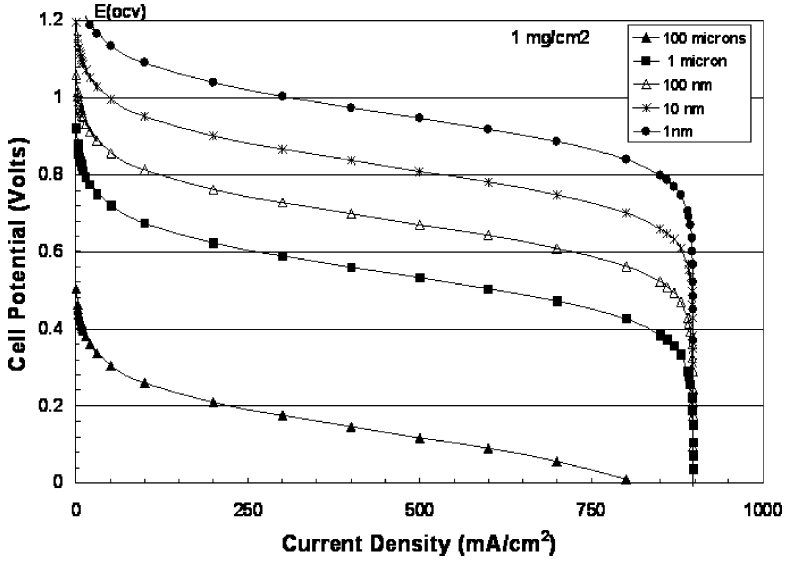

Fig. 5. Particle size effect on active surface area for a catalyst utilization coefficient of 0.2 and catalyst loading of 1 mg/cm^2.

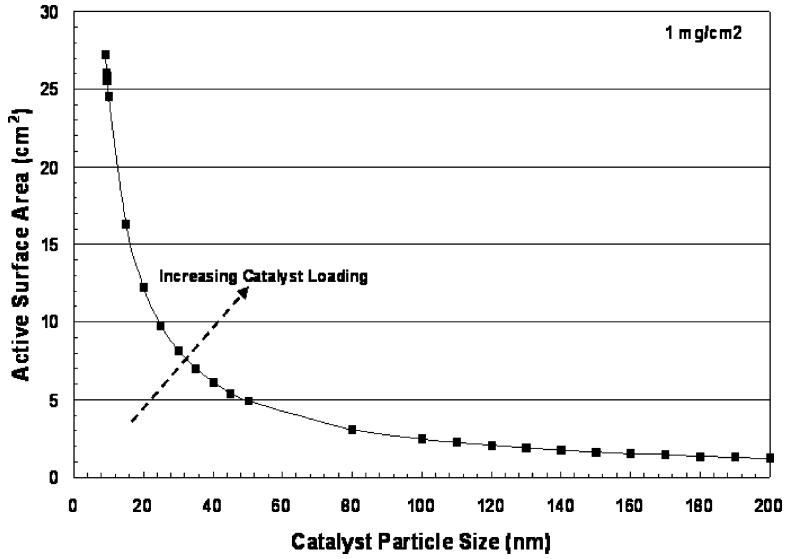

Fig. 6. Effect of Pt catalyst particle size on the cell polarization for catalyst loading of 1 mg/cm^2.

Table 1
Comparison of model predictions to experimental data

Current density (mA/cm^2)	Cell potential, experiment (volts)[a]	Cell potential, present model (volts)	Difference (%)
Pt loading: 2.64 mg/cm^2; particle size: 3.9 nm			
600	0.58	0.69	15.9
800	0.52	0.56	7.1
Pt loading: 3.96 mg/cm^2; particle size: 8.8 nm			
400	0.74	0.85	12.9
600	0.68	0.76	10.5
800	0.58	0.65	10.7
Pt loading: 5.12 mg/cm^2; particle size: 2.5 nm			
400	0.71	0.89	9.2
800	0.61	0.69	11.6

[a] Reference [33].

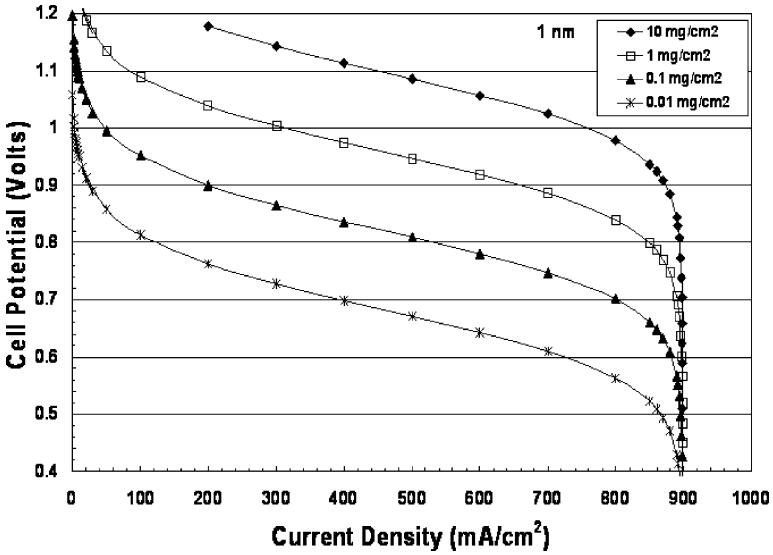

Fig. 7. Catalyst loading effect on the i–v curve in PEM fuel cell for catalyst particle size of 1 nm.

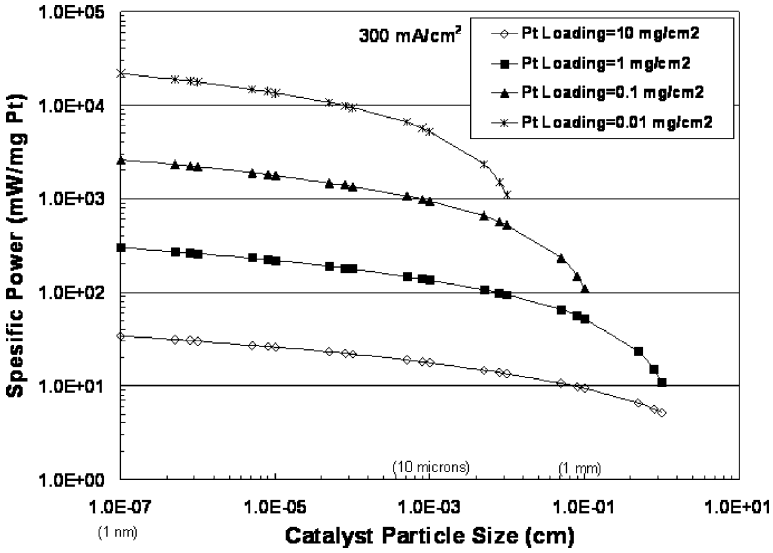

Fig. 8. PEM fuel cell specific power as a function of catalyst particle size and loading at current density of 300 mA/cm^2.

utilized in a PEM fuel cell is “intrinsic” to the random mix of components in the catalyst layer, which explains the low catalyst utilization reported in the literature [34,35]. Pt utilization, even in the best electrodes, is quit low (10–25%) [36]. The problem of low Pt utilization has been attributed to a number of reasons [27,36]: too high or too low Nafion content results in loss of connectivity of catalyst particles to membrane and diffusion layer; high PTFE content in the catalyst layer increases hydrophobicity, resulting in improved oxygen supply and product water removal at the expense of the Nafion percolation which effects the supply of protons; Pt particles located in very fine pores are not accessible to protons due to high molecular weight of Nafion and that is not able to penetrate small pores.

“On the other hand, high catalyst utilization has also been reported [38–42]. The higher catalyst utilization was attributed to more efficient catalyst layer structures and MEA preparation methods. For example, Xiaoliang et al. [38] found that the utilization of catalyst particles in the immersed and brushed E-TEK electrode is 77.8 and 22%, respectively. This shows that when the E-TEK is impregnated by immersion so that sufficient proton passageways are provided to the catalyst particles, the platinum utilization can increase to 77.8%, which is higher than that of thin-film catalyst layer.”

The present model predicts that, even if optimum connectivity and percolation are achieved, the Pt utilization will remain low due to intrinsic characteristics associated with a

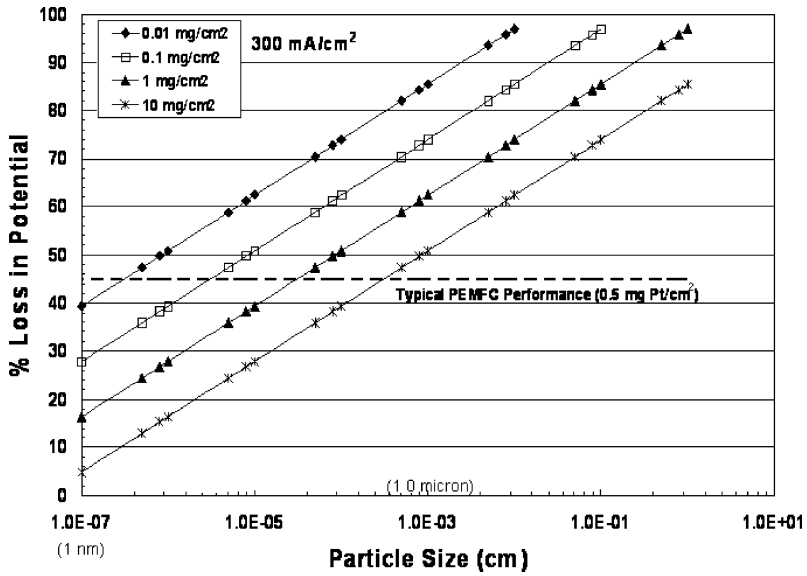

Fig. 9. Effect of particle size and loading on loss in cell voltage at current density of 300 mA/cm^2.

randomly distributed catalyst layer components. The utilization coefficient can only be raised through designing catalyst layer in a way that provides higher three-phase contact than achieved from "random" conventional mixing of catalyst components. Innovative designs and methods of applications to make better use of catalyst are needed. PEM fuel cell requires a tailored design of electrodes for optimal catalyst placement, hence, it is expected that these better-prepared catalyst layer will have higher values of γ for same catalyst loading.

The effect of catalyst utilization coefficient is illustrated in Fig. 10. A hypothetical 45% increase in cell output voltage from 0.58 to 0.84 V (at $i = 300\,\text{mA/cm}^2$) as γ is raised from 0.02 to 1. The model also allows for the determination of the utilization coefficient experimentally. A utilization map, which is active surface area, S, versus (m_c/r_c) ratio for different γ values (from Eq. (17)), is illustrated in Fig. 11. This diagram provides a valuable tool that allows the determination of γ experimentally using independently measured S, m_c and r_c. The significance of this map is that it provides a way to assist in the optimization of catalyst layer by trying different designs and testing their utilization coefficient using this map.

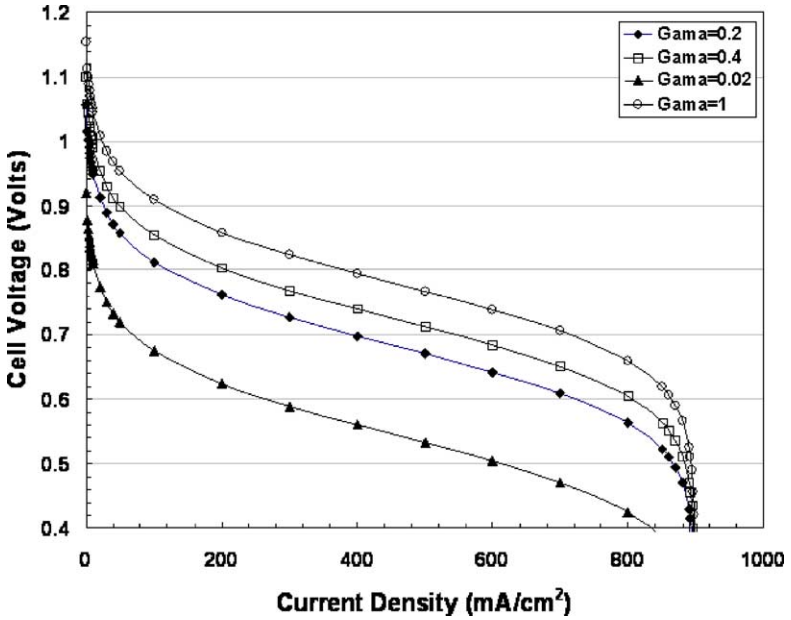

Fig. 10. The dependence of the PEM fuel cell i–v characteristics on the catalyst utilization coefficient.

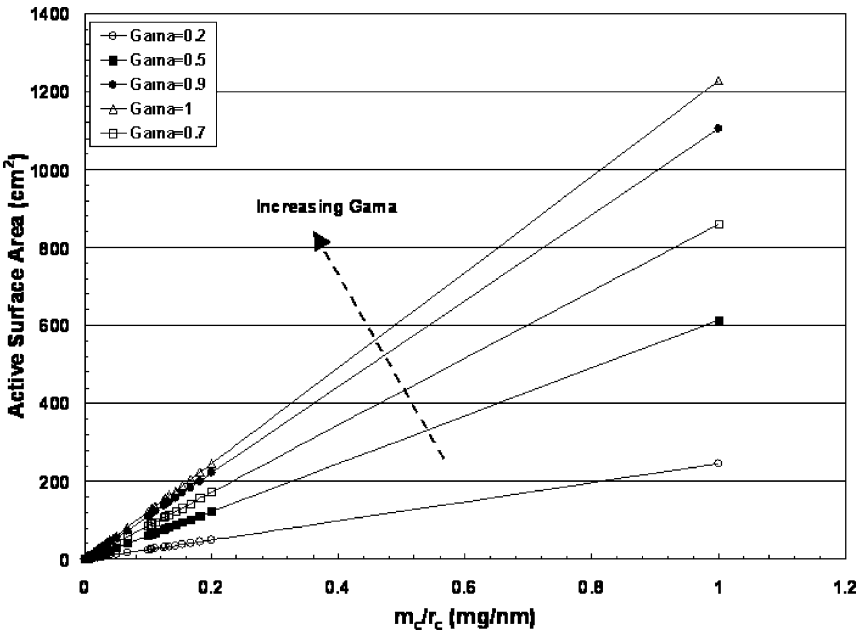

Fig. 11. Catalyst utilization map illustrating the dependence of the active surface area on the catalyst loading to particle size ration for various catalyst utilization coefficients.

5. Conclusions

- A model has been developed to relate PEM fuel cell performance to catalyst particle size, loading and utilization based on randomly distributed catalyst layer components.
- A modified Butler–Volmer equation has been developed and proved to be in good agreement with experimental data.
- The model predicts a 0.84 V increase (at 300 mA/cm^2) in cell potential as Pt particle size is reduces from 100 μm down to 1 nm.
- The model also predicts that the exchange current at 1 nm Pt particle size is three orders of magnitude higher than that at 1 μm.
- A utilization coefficient has been incorporated into the model, whose value is a function of the distribution of components in the catalyst layer.
- The model predicts an upper limit of 22% of the amount of catalyst that can be utilized in a randomly distributed catalyst layer constituents.
- Catalyst utilization can only be improved through innovative designed placement of catalyst layer components.
- A utilization map has been developed and constructed, which can be used to predict and design a catalyst microstructure that optimizes fuel cell performance.

References

[1] T.R. Jervis, L.R. Newkirk, J. Mater. Res. 1 (1986) 420.
[2] C.M. Lukehart, K.C. Kwiatkowski, J.O. Murphy, S.F. Simpson, J. Cluster Sci. 11 (3) (2000) 449.
[3] D.G. Morris, M.A. Morris, Acta Metall. Mater. 39 (8) (1991) 1763.
[4] X.D. Liu, J.T. Wang, B.Z. Ding, Scripta Metall. 28 (1993) 59.
[5] S. Bouaricha, J.P. Dodelet, D. Guay, S. Boily, R. Schulz, J. Alloys Compd. 307 (2000) 226.
[6] Z.N. Farhat, Y. Ding, D.O. Northwood, A.T. Alpas, Mater. Sci. Eng. A 206 (1996) 203.
[7] C.M. Lukehart, D.L. Boxall, G.A. Deluga, E.A. kenik, W.D. King, Chem. Mater. 13 (3) (2001) 891.
[8] J.J. Sunol, M.E. Bonneau, L. Roue, D. Guay, R. Schulz, Appl. Surf. Sci. 158 (3) (2000) 252.
[9] A. Gebert, M. Lacroix, O. Savadogo, R. Schulz, J. Appl. Electochem. 30 (9) (2000) 1061.
[10] S. Mukerjee, S.J. Lee, E.A. Ticianelli, J. McBreen, B.N. Grgur, N.M. Markovic, P.N. Ross, J.R. Giallombardo, E.S. De Castro, Electrochem. Solid State Lett. 2 (1) (1999) 12.
[11] H. Razafitrimo, M. Blouin, L. Roue, J. Huot, R. Schulz, J. Appl. Electrochem. 29 (5) (1999) 627.
[12] P. Pharkya, Z. Farhat, E. Czech, H. Hawthorne, A. Alfantazi, Hydrogen & Fuel Cells Conference, Vancouver, Canada, 8–11 June 2003.
[13] E. Czech, Z. Farhat, H. Hawthorne, A. Alfantazi, Y. Xie, The Conference of Metallurgists COM, Vancouver, Canada, 24–27 August 2003.
[14] R.F. Mann, J.C. Amphlett, B.A. Peppley, Int. J. Hydrogen Energy 21 (8) (1996) 673.
[15] J.C. Amphlett, R.M. Baumert, T.J. Harris, R.F. Mann, B.A. Peppley, P.R. Roberge, J. Electrochem. Soc. 142 (2) (1995) 1.
[16] J. Kim, S.-M. Lee, S. Srinivasan, J. Electrochem. Soc. 142 (8) (1995) 2670.
[17] S.A. Grot, K.R. Weisbrod, N.E. Vanderborgh, Electrochem. Soc. Proc. 23 (1995) 52.
[18] T.F. Fuller, J. Newman, J. Electrochem. Soc. 140 (5) (1993) 1218.
[19] C. Marr, X. Li, J. Power Sources 77 (1999) 17.
[20] T.E. Springer, T.A. Zawodzinski, S. Gottesfeld, J. Electrochem. Soc. 138 (8) (1991) 2334.
[21] D.M. Bernardi, M.W. Verbrugge, AIChE 37 (9) (1991) 1151.
[22] D.M. Bernardi, M.W. Verbrugge, J. Electrochem. Soc. 139 (9) (1992) 2477.
[23] T.V. Nguyen, R.E. White, J. Electrochem. Soc. 140 (8) (1993) 2178.
[24] K.R. Weisbrod, S.A. Grot, N.E. Vanderborgh, Electrochem. Soc. Proc. 23 (1995) 153.

[25] J.H. Lee, T.R. Lalk, A.J. Appleby, J. Power Sources 70 (1998) 258.
[26] S. Gottesfeld, T.A. Zawodzinski, Adv. Electrochem. Sci. Eng. 5 (1997) 195.
[27] M. Ekerling, A. Kornyshev, J. Electroanal. Chem. 453 (1998) 89.
[28] L. You, H. Liu, Int. J. Hydrogen Energy 26 (2001) 991.
[29] R.F. Mann, J.C. Amphlett, M.A.I. Hooper, H.M. Jensen, B.A. Peppley, P.R. Roberge, J. Power Sources 86 (2000) 173.
[30] J. Larminie, A. Dicks, Fuel Cell Systems Explained, John Wiley, UK, 2000.
[31] Kulikovsky, Fuel Cell 1 (2) (2002) 162.
[32] J. Amphlett, R. Baumert, R. Mann, B. Peppley, P. Roberge, T.J. Harris, J. Electrochem. Soc. 142 (1) (1995) 9.
[33] R. Mosdale, S. Gamburzev, O. Velev, S. Srinivasan, Electrochem. Soc. Proc. 23 (1995) 48.
[34] M. Loffler, B. Grob, H. Natter, R. Hempelmann, T. Krajewski, J. Divisek, Scripta Mater. 44 (8/9) (2001) 2253.
[35] J. McBreen, J. Electrochem. Soc. 132 (1985) 112.
[36] E. Passalacqua, F. Lufrano, G. Squadrito, A. Patti, L. Giorgi, Electrochem. Acta 46 (2001) 799.
[37] George Hoogers, Fuel Cell Technology, first ed., CRC Press, UK, 2002.
[38] C. Xiaoliang, Y. Baolian, H. Ming, Z. Jingxin, Q. Yaguang, Y. Jingrong, J. Power Sources 79 (1999) 75.
[39] S.J. Lee, S. Mukerjee, J. McBreen, Y.W. Rho, Y.T. Kho, T.H. Lee, Electrochem. Acta 43 (1998) 3693.
[40] T.R. Ralph, G.A. Hards, J.E. Keating, S.A. Campbell, D.P. Wilkinson, M. Davis, J. St Pierre, M.C. Johnson, J. Electrochem. Soc. 144 (1997) 3845.
[41] M. Watanabe, H. Uchida, M. Emori, J. Phys. Chem. B 102 (1998) 3129.
[42] S. Arico, P. Creti, N. Giordano, V. Antonucci, P.L. Antonucci, A. Chuvilin, J. Appl. Electrochem. 26 (1996) 959.